Journal of Alloys and Compounds 498 (2010) 88–94

Contents lists available at ScienceDirect

Journal of Alloys and Compounds

journal homepage: www.elsevier.com/locate/jallcom

Evolution of microstructures and textures of 7050 Al alloy hot-rolled plate during staged solution heat-treatments

Yun-Lai Deng[a,b,*], Li Wan[a,b], Yong Zhang[a,b], Xin-Ming Zhang[a,b]

[a] School of Materials Science and Engineering, Central South University, Changsha 410083, China
[b] Key Laboratory of Nonferrous Materials Science and Engineering, Ministry of Education, Changsha 410012, China

ARTICLE INFO

Article history:
Received 13 October 2009
Received in revised form 10 March 2010
Accepted 13 March 2010
Available online 18 March 2010

Keywords:
7050 Al alloy
Solution
Rolling
Recrystallization
Microstructure
Texture

ABSTRACT

The evolution of the microstructures and textures of 7050 Al alloy hot-rolled plates were studied during a series of staged solution heat-treatments (S-SHT). The results show that the texture type in the specimens after various S-SHT processes is similar to that of the as hot-rolled for solution temperatures up to 490 °C. The grain orientations are assembled to typical β-fiber and α-fiber, together with some {0 0 1} ⟨1 0 0⟩ texture. The orientation densities of {1 2 4} ⟨2 1 1⟩ and {1 1 2} ⟨1 1 1⟩ textures in the S-SHT specimens are higher than that of the as hot-rolled; however, they decrease with increasing solution temperature because of recovery and continuous recrystallization. At 475 °C, the specimens contain Al_2CuMg and Al_7Cu_2Fe particles, but only Al_7Cu_2Fe particles exist at 490 °C. The S-SHT described in this paper improves the mechanical properties of 7050 Al alloy plate, in particular, the elongation to failure, which increases from 8.8% to 14.2%.

1. Introduction

Al–Zn–Mg–Cu (7000 series) Al alloy plates are widely used in the aeronautical and aerospace industries because of their excellent mechanical properties and low density [1]. The properties of these alloys can be optimized by applying a series of treatments, including solution, quenching, and aging heat-treatments [2,3]. Aging heat-treatment is an important final step in the process. The relationships between microstructures and properties after multi-stage aging, pre-deforming, and over-aging, have been documented in literatures [4–7]. Solution heat-treatment (SHT) is also widely studied. The 7000 series aluminum alloys need to be solution heat-treated at a high temperature to dissolve coarse secondary-phase particles (>1 μm) and to facilitate the precipitation of the enhancing phases produced subsequently. However, a solution process at high temperatures would lead to recrystallization and to a decrease in the strength, toughness, and even resistance to corrosion of the aged materials [8–10]. Previous literatures have reported that the deformed 7050 Al alloy materials were generally heated to 470–480 °C during SHT [8,11–14]. The effects of textures in 7050 Al alloy plate on deformation behavior and properties have also been reported [15–17], but the development of texture in 7050 Al alloy plates during heat-treatment has received little attention to date, in particular with respect to recrystallization microstructures. It is therefore very necessary to systemically clarify the evolution of microstructures and textures of 7050 Al alloy plate during SHT.

The present work investigated the microstructures and textures in specimens heated by a series of staged SHT (S-SHT) processes, with the temperature increasing from 150 °C to 520 °C. The aim of this study was to determine the relationship between the microstructures and the textures in a 7050 Al alloy hot-rolled plate during S-SHT, and subsequently to modify the SHT to improve the Al alloy properties.

2. Experimental

The chemical composition of the 7050 Al alloy hot-rolled plate used in this study is shown in Table 1. The total rolling reduction of the plate was 80%. In order to avoid inhomogeneous microstructures and textures along the normal direction of the thick plate, all specimens were taken from the center of the corresponding plate. The dimensions of the specimens were 3 mm (normal direction) × 10 mm (transverse direction) × 15 mm (rolling direction). The specimens were heated according to the schedule parameters specified in Table 2, and the heated specimens were immediately quenched in water at room temperature. Because the thickness of the specimens is small, the heating and cooling rates at different positions of the specimens can be treated as uniform.

Optical micrographs (OMs) of the specimens were etched by Graff Sargent agent (1 ml HF + 16 ml HNO3 + 3 g CrO3 + 83 ml water). The areas where no recrystallization took place have high concentrations of sub-grains and appear dark in the OMs after etching. In contrast, the recrystallization grains do not contain sub-grains and appear bright after etching. As a consequence, the recrystallization areas in the OMs can be determined according the percentage of the bright area or dark area. Hardness measurements were carried out by using a load of 3 kg and a holding time

* Corresponding author at: School of Materials Science and Engineering, Central South University, Changsha 410083, China. Fax: +86 731 88876913.
E-mail address: dengylcsu@126.com (Y.-L. Deng).

0925-8388/$ – see front matter.
doi:10.1016/j.jallcom.2010.03.117

Table 1
Chemical composition (wt.%) of the investigated 7050 Al alloy plate.

Zn	Mg	Cu	Zr	Fe	Si	Others (single)	Al
6.23	2.35	2.26	0.11	0.12	0.08	≤0.05	Bal.

Table 2
Schedule parameters of the staged SHT.

Number of SHT	Schedule parameters of SHT
S150	150 °C/12 h
S200	S150 + 200 °C/12 h
S300	S200 + 300 °C/12 h
S400	S300 + 400 °C/12 h
S465	S400 + 465 °C/4 h
S475	S400 + 475 °C/4 h
S490	S400 + 490 °C/4 h
S520	S400 + 520 °C/2 h

of 15 s. The microstructures were observed with a JSM-6360LV scanning electron microscopy (SEM) and a TECNAIG^2 20 transmission electron microscope (TEM). The phase determination was carried out by a Rigaku D/Max 2500 type X-ray diffraction (XRD) apparatus. The mechanical properties were determined using a CSS44100 electronic testing machine at a strain rate 1×10^{-3} s^{-1}. The tensile specimens with dimension of 4 mm diameter and a gauge length of 6 mm were cut from the plate along the normal direction.

In order to analyze texture components in a specimen, four incomplete pole figures—{1 1 1}, {2 0 0}, {2 2 0}, and {3 1 1}—were measured by the reflection Schulz method using a Brucker D8 Discovery. The experimental orientation distribution function (ODF) was computed according to a series expansion method (l_{max} = 34, including the even and odd terms) [18].

3. Results and analyses

3.1. Microstructures and textures

Fig. 1 shows representative optical micrographs of the specimens treated by different S-SHT processes. It can be seen that the fraction of the bright areas increases as the solution temperature increases from 400 °C to 520 °C, indicating that recrystallization occurs in conjunction with increasing temperature. Furthermore, although the recrystallization grains become equiaxed in the S520 specimen, the elongated grains are retained in the S400, S475, and S490 specimens, indicating that the motion of high-angle grain boundaries does not occur significantly during S-SHT until the solution temperature reaches 490 °C.

Table 3
Texture components discussed in present paper (approximated).

Notation	Miller indices {h k l} ⟨u v w⟩	Euler angles		
		φ_1	Φ	φ_2
G-	{0 1 1} ⟨1 0 0⟩	0°	45°	0°/90°
B-	{0 1 1} ⟨2 1 1⟩	35°	45°	0°/90°
R-	{1 2 4} ⟨2 1 1⟩	55°	30°	65°
S-	{1 2 3} ⟨6 3 4⟩	60°	40°	65°
C-	{1 1 2} ⟨1 1 1⟩	90°	30°	45°
Cube	{0 0 1} ⟨1 0 0⟩	0°	0°	0°/90°

Fig. 2 shows the ODF graphics for the specimens as hot-rolled plate and after various S-SHT processes. The levels of orientation density are ($f(g)$): 1.0, 3.0, 6.0, 9.0, 12.0, 15.0. The textures in the hot-rolled specimen (Fig. 2(a)) are comprised of orientations that are typical for plane strain compress (PSC) of F.C.C. metal Al and Al alloys, which are listed in Table 3. Here, most orientations are assembled to the β-fiber that covers Euler-angle space from {1 1 2} ⟨1 1 1⟩ (C-), through {1 2 4} ⟨2 1 1⟩ (R-) or {1 2 3} ⟨6 3 4⟩ (S-), to {0 1 1} ⟨2 1 1⟩ (B-) orientations. The S- and R- orientations are similar. Generally, the S- texture occurs in PSC, the R- occurs in recrystallization (e.g. Ref. [19]). This texture type along the β-fiber is in good agreement with the previous works about 7010 Al alloy hot-rolled plate [20]. The textures in the specimens treated by S-SHT (Fig. 2(b)–(d)) are similar to those in the as hot-rolled, but the effect of S-SHT on development of textures can be observed by orientation fibers in Fig. 3.

Fig. 3 sketches the α-fiber, β-fiber, and the Cube_RD and Cube_ND fibers of the ODFs illustrated in Fig. 2. These fibers are more convenient to compare the development of the texture components than that in ODF graphics (Fig. 2). It can be seen that the $f(g)$ data along the β-fiber at φ_2 = 65° is laid near the R- orientation. The orientation densities of the R- and C- textures in the S475, S490 and S520 specimens are higher than that of the hot-rolled one; however, the orientation densities of the R- and C- textures in the specimens after S-SHT decrease with increasing solution temper-

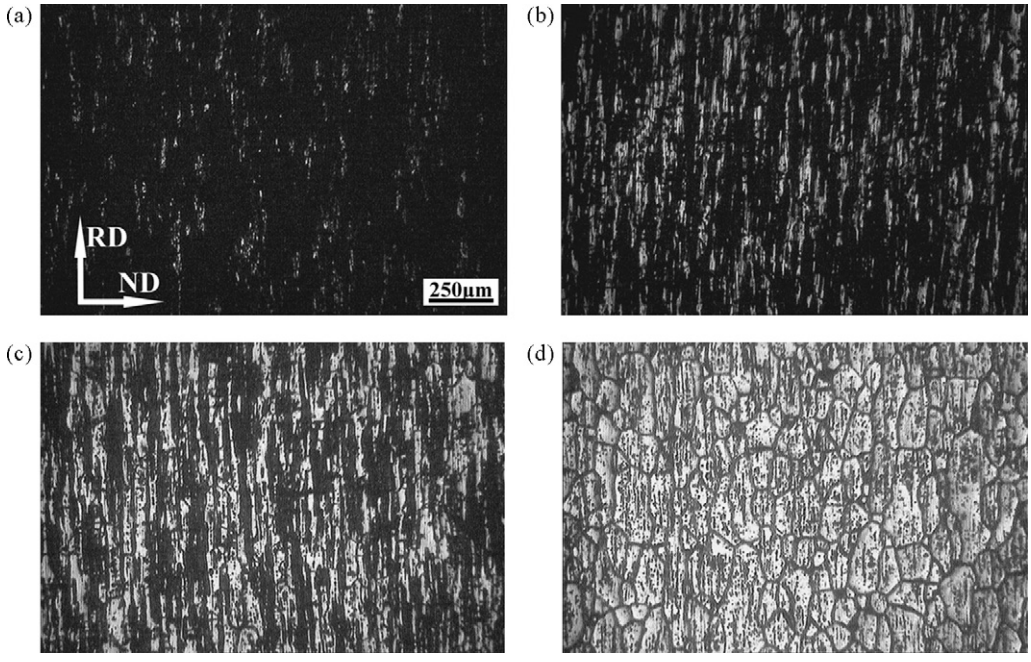

Fig. 1. Optical micrographs of recrystallization microstructures (the white zone) of the specimens for solution temperatures of (a) 400 °C, (b) 475 °C, (c) 490 °C, and (d) 520 °C.

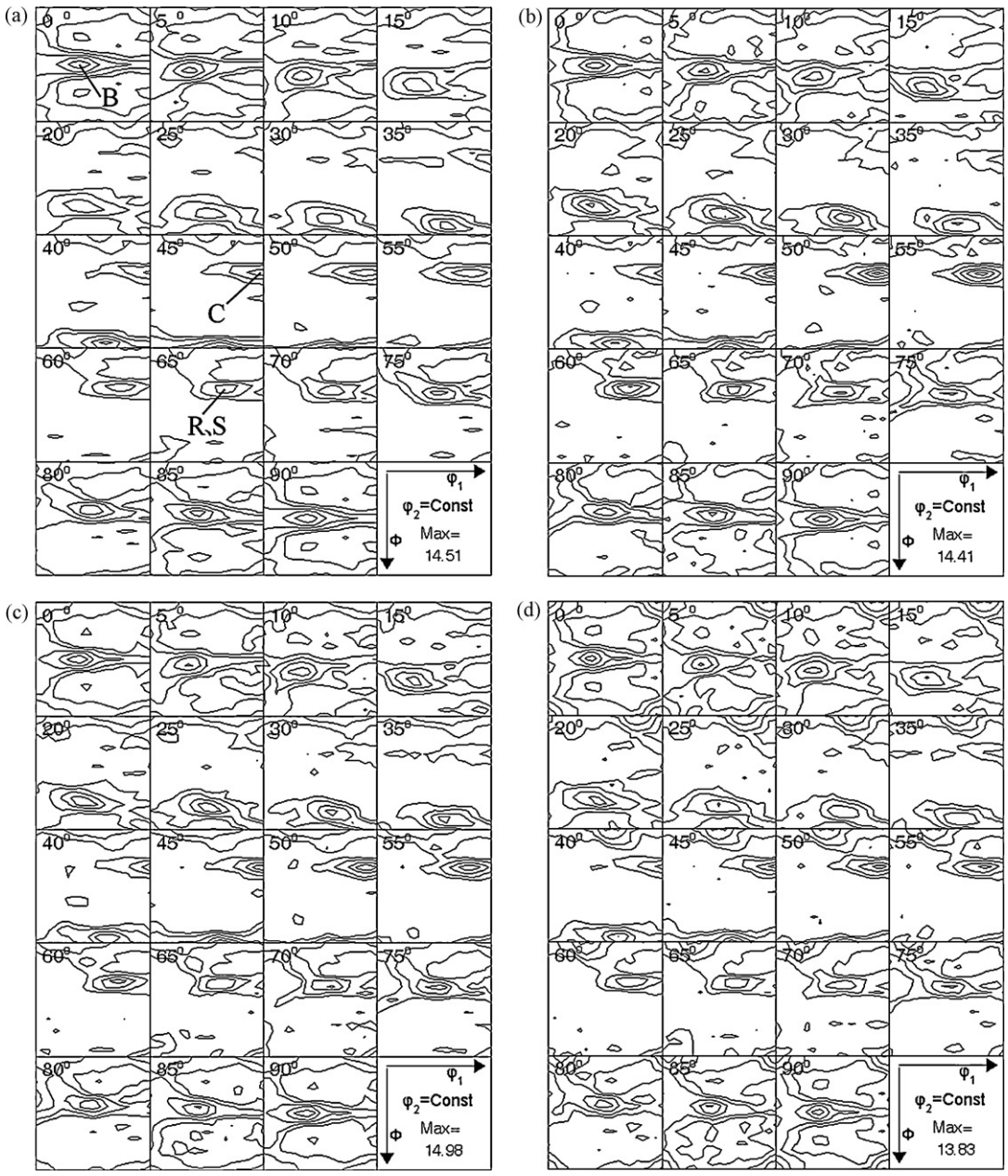

Fig. 2. Orientation distribution functions (ODFs) of (a) the rolled specimen and the S-SHT specimens (b) S475, (c) S490 (c), and (d) S520.

atures. There is little difference between the orientation densities of the textures on α-fiber, i.e., the {0 1 1} ⟨1 0 0⟩ (G-) and B- textures, in the S-SHT specimens and in the hot-rolled one. The B-texture has the maximum $f(g)$. The Cube_RD and Cube_ND fibers represent the orientation density distribution of the Cube texture rotating along the rolling direction (RD) and the normal direction (ND), respectively. The Cube texture increases noticeably only in the S520 specimen, which will be discussed in Section 3.3.

The formation mechanism of the recrystallization microstructures and textures in the deformed F.C.C. Al and Al alloy is complicated during annealing. The terms of continuous recrystallization (extended recovery) and discontinuous recrystallization are usually used to describe textures and microstructures associated with recrystallization phenomena (e.g. Refs. [19] and [21]). The orientation distributions of the newly equiaxed grains formed by discontinuous recrystallization are much different from that of the deformed matrix, such as Cube texture. However, when the continuous recrystallization occurs, the grain morphology maybe the lamellar and/or the equiaxed grains, but the rolling texture type is remained with little change. The evolution of the textures described above reveals that textures in the specimens treated with various S-SHT processes are similar to those of the hot-rolled until the solution temperature reaches at 520 °C. In short words, the continuous recrystallization mainly occurs during the present S-SHT processes, although the lamellar recrystallization grains remain along the rolling direction are observed in Fig. 1(a)–(c), and the equiaxed grains are observed in Fig. 1(d). Because the range of the rolling temperature of the present hot-rolled plate before SHT was 350–450 °C, the characterization of the textures in the S-SHT specimens should be explained by the effects of randomization of the texture by particle stimulated nucleation (PSN) and the texture sharpening by continuous recrystallization, as is revealed as the hot-deformation 7010 Al alloy by Engler et al. and Morere et al. [20,22]. In present work, it is clear that the sharpness of the C-

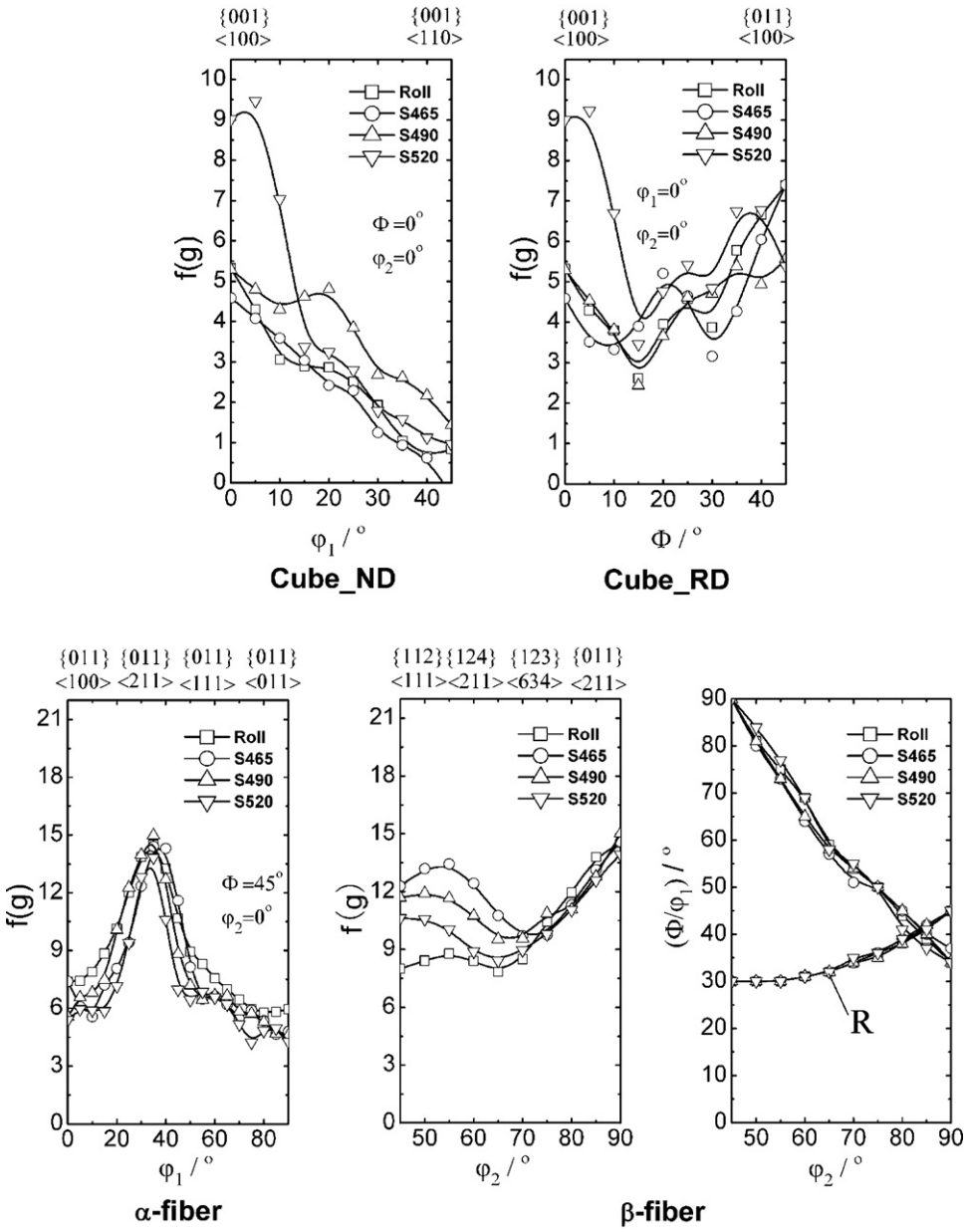

Fig. 3. Orientation fibers of the ODFs in Fig. 2.

and R- textures along the β-fiber is dominant even for the S520 specimen.

Furthermore, there is little change in the orientation densities of the B- and G- textures along the α-fiber, which can be explained by their smaller Taylor factor and lower deformation-stored energy during rolling deformation, which means less driving force for recovery and recrystallization. While the increase of orientation densities of the C- and R- textures can be explained by their larger Taylor factors and higher deformation-stored energy during deformation, which means more driving force for recovery and recrystallization. As a result, these textures along β-fiber become sharp.

3.2. Coarse secondary-phase particles

The S465, S475, S490, and S520 specimens were investigated by SEM and by energy diffraction spectrum (EDS) analysis. Fig. 4 shows an image of typical microstructures observed by SEM using the back scatter electron image technique. The coarse secondary-phase particles can be identified by combining the results of the EDS and XRD methods.

The morphology of the coarse secondary-phase particles in the S465 specimen is shown in Fig. 4(a). The particles appear polygonal or globular. The results of EDS (Fig. 5) and XRD (Fig. 6) indicate that the polygonal particles are Al_7Cu_2Fe (Fe-rich phase) and that the globular particles are $Al_5Cu_6Mg_2$ or Al_2CuMg (the two phases are denoted S1 and S, respectively). Because the amount of the Al_7Cu_2Fe phase is small, it was not easily identified by XRD. The morphology of the coarse secondary-phase particles in the S475 specimen is shown in Fig. 4(b). The majority of these particles are in the S phase, as can be verified from the diffraction scratch containing the diffraction peaks of the S phase. The S1 phase is a non-equilibrium precipitation phase during hot-rolling, and is much more easily dissolved, so that little of it remains. The morphology of the coarse secondary-phase particles in the S490 specimen is shown in Fig. 4(c). No S phase has been found by SEM or XRD as a result of the S phase being dissolved. The morphology of the coarse secondary-phase particles in the S520 specimen

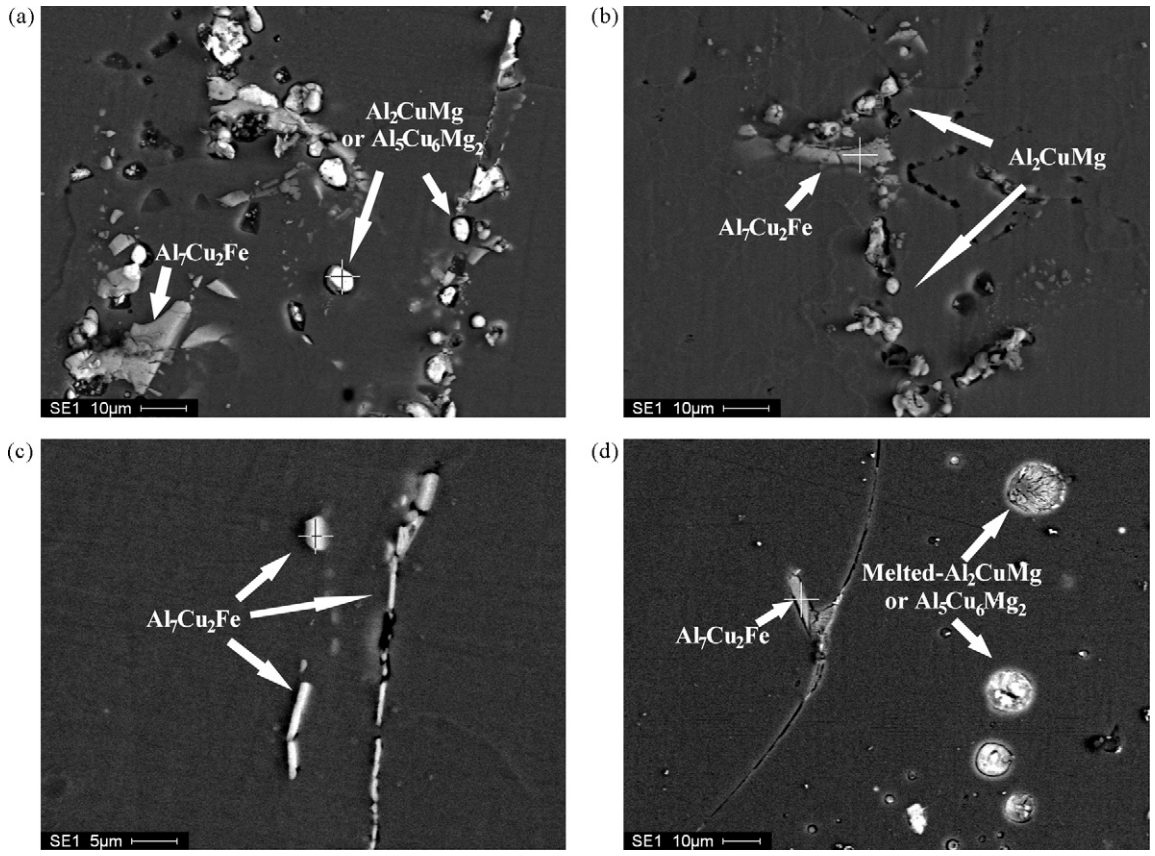

Fig. 4. Backscattered electron images of the S-SHT specimens (a) S465 (b) S475 (c) S490 (d) S520.

is shown in Fig. 4(d). It can be seen that the S or S1 existed in a spherical morphology and Fe-rich phases existed in polygonal morphology with distinct edges and corners.

3.3. TEM micrographs

Fig. 7 shows the microstructures of the specimens observed by TEM. The hot-rolled sub-grains can be distinguished even though the inhomogeneous stress field in the hot-rolled specimen decreases the clarity of the TEM observations in Fig. 7(a). Fig. 7(b) shows the sub-grains as clearly visible in the S200 specimen. The dislocations disencumber from pining of the secondary-phase particles. The density of dislocations decreases by dislocation counteracting. The contrasts within sub-grain regions appear uniform; a typical sub-microstructural feature of recovery. Another important feature is the precipitation of nanometer-scale secondary-phase particles discontinuously along the grain or sub-grain boundaries. Both sides of the grain and sub-grain boundaries form precipitation-free zones (PFZs). The precipitated particles are expected to be $MgZn_2$ phase.

Fig. 7(c) shows the sub-grains becoming uniformly oriented in the S300 specimen. The $MgZn_2$ particles precipitated along the grain or sub-grain boundaries begin to dissolve into the matrix. The sub-grain boundaries become blurred as the sub-grains merge (marked A). The trajectory of the sub-grain boundaries can also be followed (marked B). The secondary-phase particles can be seen at

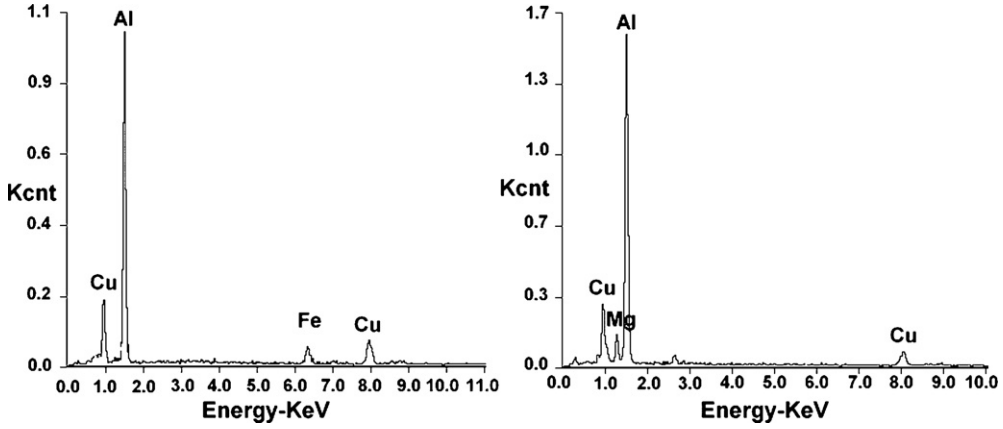

Fig. 5. Energy diffraction spectrum (EDS) of coarse secondary-phase particles.

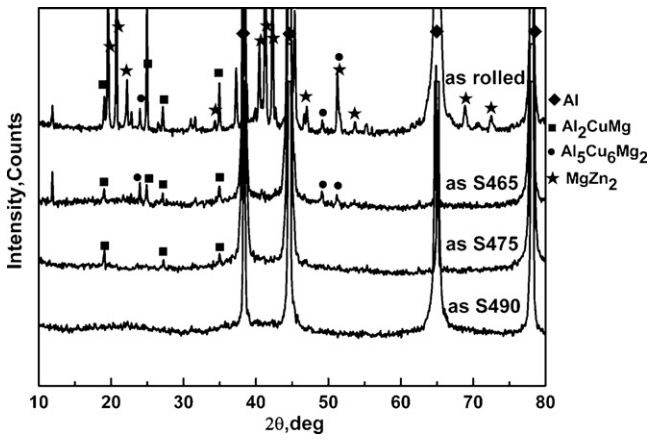

Fig. 6. X-ray diffraction (XRD) patterns of the investigated specimens.

the sub-grain boundaries and within the sub-grain (marked C). It is worthy to notice the misorientation degree of the matrix surround these particles is less than 15°.This at least suggests a probable mechanism: during the present S-SHT process with an average heating rate slower than 0.1 °C/min in the range of 150–300 °C, the dissolution rate of the $MgZn_2$ phase particle is faster than that of the recrystallization by PSN.

The trajectories of the merging sub-grains with similar contrast, i.e., with very small orientation deviations (marked A), and of sub-grain boundaries (marked B) can both be observed in the S490 specimen, as illustrated in Fig. 7(d). Except for growing sub-grains, partial sub-grains are separated by high-angle boundaries (marked C). The small crystalline with high-angle boundaries suggests a nucleation of discontinuous recrystallization. The cube orientation nucleation would develop in the matrix when continuous recrystallization occurs at lower temperature. And then, if annealing followed at higher temperature, the cube texture would develop by discontinuous recrystallization, which can explain that the cube texture increases noticeably in the S520 specimen. The similar development of the cube texture has been found in high purity Al foils [19].

3.4. Effect of S-SHT on the mechanical properties of 7050 Al alloy plate

The microstructural and textural features described above indicate that the current S-SHT process, where the temperature is increased to 490 °C, successfully dissolves coarse particles into the matrix, thereby leaving continuous lamellar recrystallization grains in the specimens. How they affected the mechanical properties of the 7050 Al alloy thick plate along the normal direction, which is generally lower than that of others directions, was investigated through tensile test. Table 4 shows the variation in the mechanical properties of tensile specimens resulting from different schemes denoted S465, S475, and S490. Both the strength and the maximum elongation before failure are improved by S-SHT. The sensitivity of

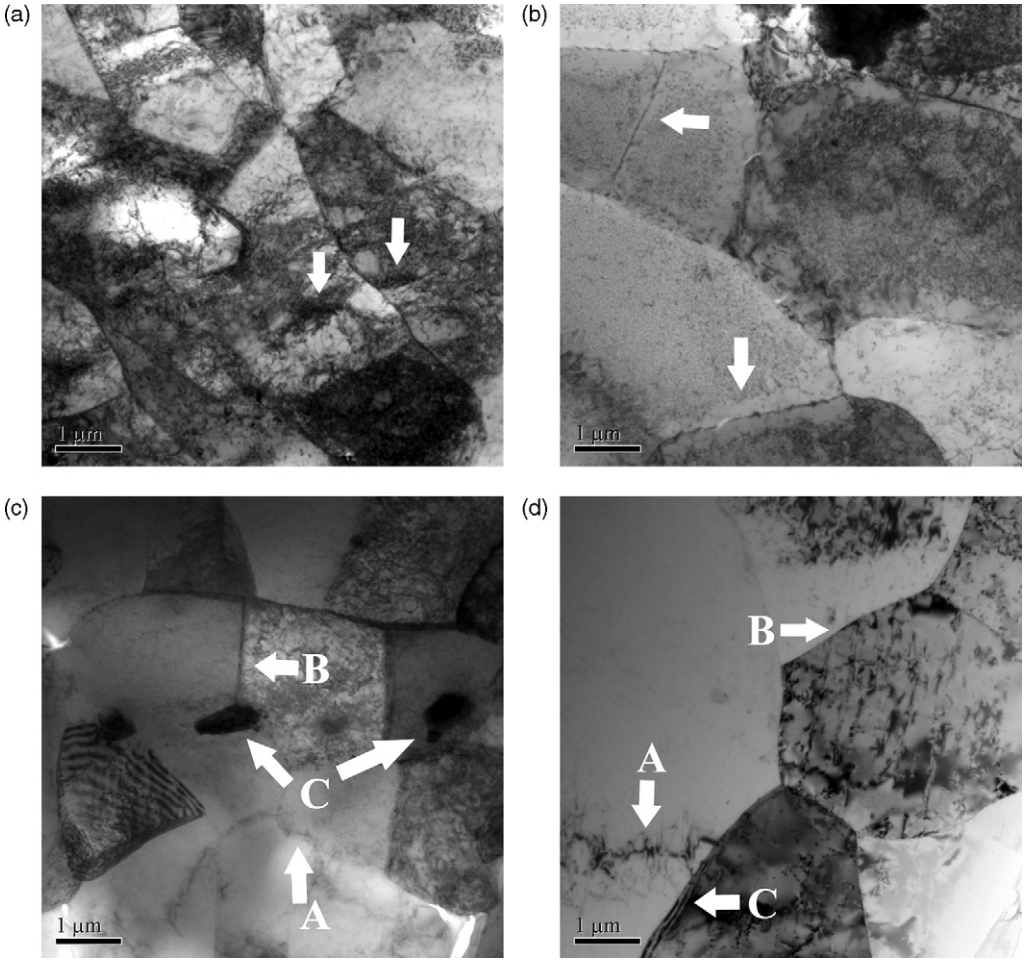

Fig. 7. Transmission electron microscopy (TEM) images of specimens (a) the hot-rolled, (b) S200, (c) S300, (d) S490.

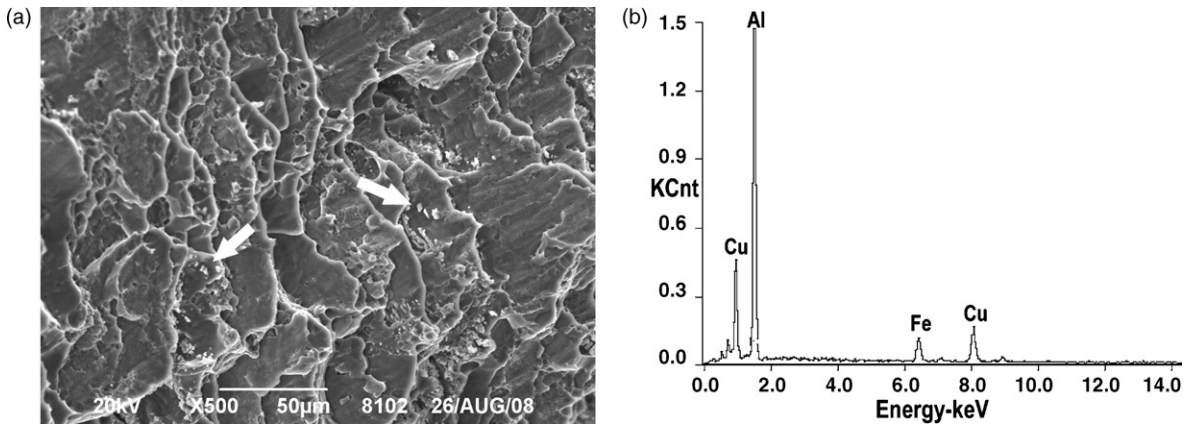

Fig. 8. (a) Fracture surface of the tensile-tested specimen observed along the normal direction of the thick plate obtained by the S490 scheme, and (b) the EDS result of the secondary-phase particles.

Table 4
Effect of solution heat-treatment on the mechanical properties of 7050-T4.

Solution treatment schemes	σ_b (MPa)	$\sigma_{0.2}$ (MPa)	δ_5 (%)
S465 (S–T)	396	285	8.8
S475 (S–T)	402	291	10.5
S490 (S–T)	415	303	14.2

these parameters is particularly notable in the elongation to failure, which increases from 8.8% (for S465) to 14.2% (for S490), i.e., by more than 50%.

Fig. 8 shows a fracture surface morphology of a failure specimen S490. It is observed that there are some coarse particles on a rough surface (indicated by an arrow in Fig. 8(a)). The surface consists of many tough nests with dimensions smaller than that of grains. These particles are determined as Fe-rich phase by EDS analysis (Fig. 8(b)), which locates at nest's bottom, which agrees well with the observation in Fig. 4(c). This reveals that the fracture model appears to be a typical tough intersubgranular model. Because a huge amount of coarse particles of the S and Fe-rich phases are included in the specimens as the S465 and S475, which hardly contributes to the strength and damage elongation, their mechanical properties are lower than that of the specimen S490.

4. Conclusions

Hot-rolled 7050 Al alloy plates were solution heat-treated following a staged schedule (S-SHT). For solution temperatures up to 490 °C, the microstructures, textures, and mechanical properties of the samples display the following patterns:

1. The morphology of recrystallization grains in the solution heat-treated plate remains lamellar with the long axis parallel to the rolling direction. The textures of the hot-rolled 7050 Al alloy plate change very little after S-SHT. The grain orientations are assembled to β-fiber and α-fiber. The orientation densities of the $\{1\,2\,4\}\langle 2\,1\,1\rangle$ and $\{1\,1\,2\}\langle 1\,1\,1\rangle$ textures in the solution heat-treated specimens are higher than that of the as hot-rolled, but they decrease with increasing solution temperature. The microstructures and textures evolve mainly by recovery and continuous recrystallization.
2. During the present S-SHT process, only texture sharpening within the continuous recrystallization matrix is verified, the dissolution of the $MgZn_2$ phase particle probably reduce the effect of randomization of the texture by particle stimulated nucleation.
3. The S-SHT process developed in this paper successfully dissolves coarse particles into matrix. For temperatures up to 475 °C, the specimen contains Al_2CuMg and Al_7Cu_2Fe particles, but only Al_7Cu_2Fe particles exist in the specimen when the temperature is raised to 490 °C.
4. Both the tensile strength and the elongation before failure, for a 7050 Al alloy thick plate, are improved by the S-SHT. Notably that the elongation to failure increases by more than 50%, from 8.8% to 14.2%, along the normal direction.

Acknowledgements

The authors gratefully acknowledge the financial support by the National Basic Program of China (No.2005CB623700).

References

[1] A. Heinza, A. Haszler, C. Keidel, S. Moldenhauer, R. Benedictus, J. Mater. Sci. Eng. A 280 (2000) 102–107.
[2] P. Archambault, D. Godard, J. Scripta Mater. 42 (2000) 675–680.
[3] D. Dumont, A. Deschamps, Y. Brechet, J. Acta Mater. 51 (2003) 713–729.
[4] D. Wang, D.R. Ni, Z.Y. Ma, J. Mater. Sci. Eng. A 494 (2008) 360–366.
[5] J.C. Lin, H.L. Liao, W.D. Jehng, C.H. Chang, S.L. Lee, J. Corros. Sci. 48 (2006) 3139–3156.
[6] C.K. Lin, S.T. Yang, J. Eng. Fract. Mech. 59 (1998) 779–795.
[7] B. Cai, B.L. Adams, T.W. Nelson, J. Acta Mater. 55 (2007) 1543–1553.
[8] J.D. Robson, J. Mater. Sci. Eng. A 382 (2004) 112–121.
[9] H.C. Fang, K.H. Chen, H. Chao, G.S. Peng, J. Corros. Sci. 51 (2009) 2872–2877.
[10] B. Morere, C. Maurice, R. Shahani, J. Driver, J. Metall. Mater. Trans. A 32A (2001) 625–632.
[11] C.S. Paglia, K.V. Jata, R.G. Buchheit, J. Mater. Sci. Eng. A 424 (2006) 196–204.
[12] G. Sha, A. Cerezo, J. Acta Mater. 52 (2004) 4503–4516.
[13] L.J. Zheng, H.X. Li, M.F. Hashmi, C.Q. Chen, Y. Zhang, M.G. Zeng, J. Mater. Process. Technol. 171 (2006) 100–107.
[14] G. Sha, A. Cerezo, J. Acta Mater. 53 (2005) 907–917.
[15] X.Y. Wang, H.E. Hu, J.C. Xia, J. Mater. Sci. Eng. A 515 (2009) 1–9.
[16] S.C. Chang, Q.D. Jiang, J.R. Hu, F.R. Chen, J. Scripta Mater. 39 (1998) 583–588.
[17] W. Robert, D. Piot, F. Eberl, J.H. Driver, J. Mater. Sci. Forum 396–402 (2002) 356–370.
[18] H.J. Bunge, Mathematische Methoden der Texturanalyse, Akademie-Verlag, Berlin, 1969.
[19] O. Engler, M.Y. Huh, J. Mater. Sci. Eng. A 271 (1999) 371–381.
[20] O. Engler, E. Sachot, J.C. Ehrstrom, A. Reeves, R. Shahani, J. Mater. Sci. Technol. 12 (1996) 717–725.
[21] F.J. Humphreys, M. Hatherly, Recrystallization and Related Annealing Phenomena, second ed., Elsevier Science Ltd., Oxford, 2004.
[22] B. Morere, C. Maurice, J. Driver, R. Shahani, J. Mater. Sci. Forum 217–222 (1996) 517–522.